

Supporting Information

Quantification of multivalent interactions between sialic acid and influenza A virus spike proteins by single molecule force spectroscopy

Jose Luis Cuellar-Camacho^{*,a}, Sumati Bhatia^{*,a}, Valentin Reiter-Scherer^b, Daniel Lauster^{a,c}, Susanne Liese^d, Jürgen P. Rabe^b, Andreas Herrmann^c and Rainer Haag^a

^aInstitute of Chemistry and Biochemistry, Freie Universität Berlin, Takustraße 3, 14195 Berlin, Germany

^bDepartment of Physics & IRIS Adlershof, Humboldt-Universität zu Berlin, Newtonstraße 15, 12489 Berlin, Germany

^cInstitute for Biology & IRI Life Sciences, Humboldt-Universität zu Berlin, Invalidenstraße 42, 10115 Berlin, Germany

^dDepartment of Mathematics, University of Oslo, Moltke Moes vei 35, 1053 Oslo, Norway

Table of Contents

1. Synthesis and characterization	2
1.1 Scheme for the synthesis of PEG linked multivalent sialoside .. Error! Bookmark not defined.	
1.2 dPGSAN ₃ 3	3
1.3 LAPEGNH ₂ 6	4
1.4 dPGSA-PEG-LA 7	Error! Bookmark not defined.
1.5 Scheme for the synthesis of PEG-linked multivalent control compound	5
1.6 LA-PEG-N ₃ 10	6
1.7 dPGOH-PEG-LA 13	7
1.8- NMR Spectra.	7
2. Sample preparation	100
2.1 Virus preparation.	100
2.2 Immobilization of influenza A virus.	100
2.3 Immobilization of poly-histidine tagged N2 proteins on NTA surfaces.	111
2.4 SFM tip functionalization.	111
3. SFM imaging and force spectroscopy	122

3.1 Scanning force microscopy.....	122
3.2 Force spectroscopy measurements.....	122
4. PeakForce imaging results.	144
4.1 Influenza A virions and protein coated surfaces.....	144
5. Force spectroscopy.	17
5.1 Quantification of unbinding forces for single and multiple monovalent-SA receptors with H3 proteins on the influenza A virus and on N2 coated surfaces.....	17
5.2 Single apparent bond.....	19
5.3 Quantification of unbinding forces for multivalent-SA receptor with Influenza A virus and N2 proteins.....	24
References	25

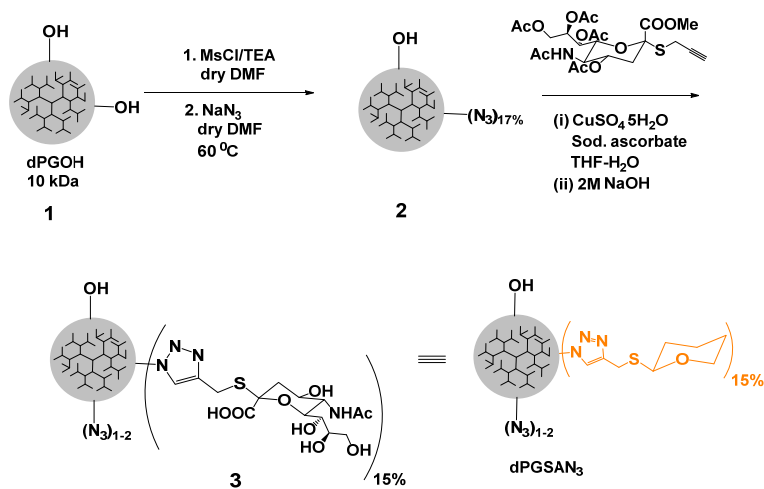
1. Synthesis and characterization

All reagents and solvents were purchased from commercial suppliers and used without further purification. Reactions requiring dry or oxygen-free conditions were carried out under argon in Schlenk glassware. ¹H NMR spectra were recorded on Bruker AMX 500 (500 MHz) and Delta Joel Eclipse 700 (700 MHz) spectrometer at 25 °C and calibrated by using the deuterated solvent peak. Infrared (IR) spectra were recorded with a Nicolet AVATAR 320 FT-IR 5 SXC (Thermo Fisher Scientific, Waltham, MA, USA) with a DTGS detector from 4000 to 650 cm⁻¹. A TSQ 7000 (Finnigan Mat) instrument was used for ESI measurements and a JEOL JMS-SX-102A spectrometer was used for the high-resolution mass spectra. Molecular weight distributions were determined by means of GPC coupled to a refractive index detector (RI) for obtaining the complete distribution (Mn, Mp, Mw, dispersity). Measurements were carried out under highly diluted conditions (5 mg/ml) from a GPC consisting of an Agilent 1100 solvent delivery system with pump, manual injector, and an Agilent differential refractometer. Three 30 cm columns (PPS: Polymer Standards Service GmbH, Germany; Suprema 100 Å, 1000 Å, 3000 Å with 5 and 10 µm particle size) were used to separate aqueous polymer samples using water with 0.1 N NaNO₃ as the mobile phase at a flow rate of 1 ml/min. The columns were operated at room temperature (rt) with the RI detector at 50 °C. The calibration was performed by using certified standards pullulan (linear) from PSS. WinGPC Unity from PSS was used for data acquisition and interpretation. Naturally occurring sialic acids constitute a family of more than 50 structurally distinct nine-carbon 3-deoxy-ulosonic acids, the most widespread derivative being 5-*N*-acetyl-neuraminic acid (Neu5Ac). We used the abbreviation of sialic acid

(SA) for Neu5Ac. Heterobifunctional PEG (MW=5 kDa) was purchased from Rapp polymere GmbH.

1.1 Synthesis of PEG linked multivalent sialoside dPGSA-PEG-LA 7

(a)



(b)

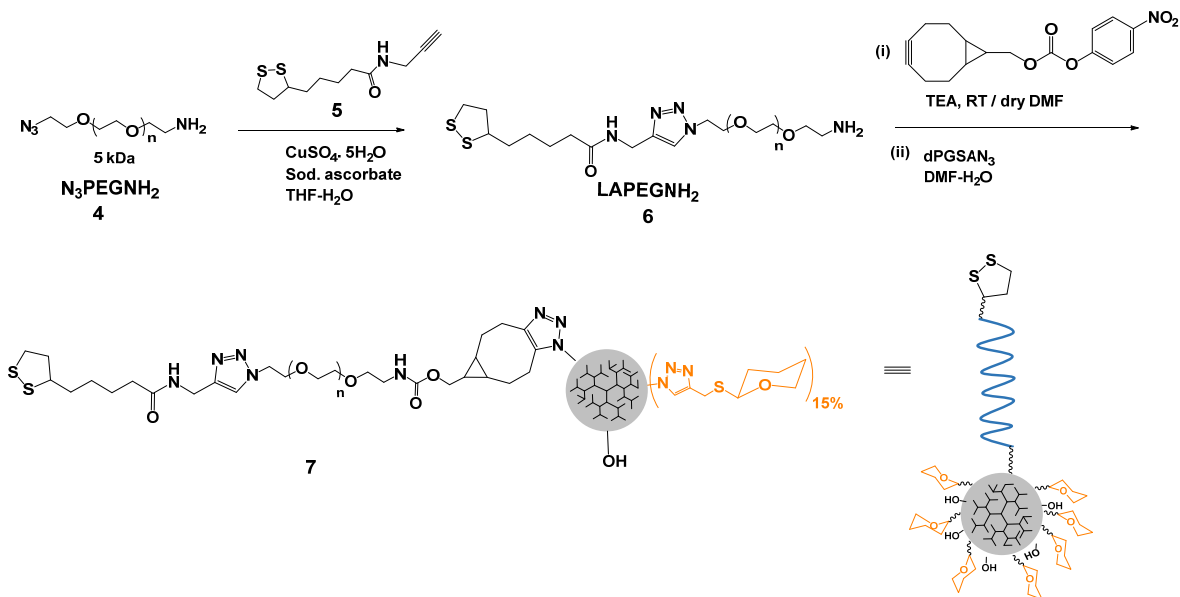


Figure S1. (a) Synthesis of multivalent sialoside dPGSAN₃. (b) Synthesis of multivalent sialoside system linked with the thioctic acid functionalized PEG linker (dPGSA-PEG-LA)

1.2 dPGSAN₃ **3**

For the preparation of dPGSAN₃ **3**, first dPGN₃ (DF = 17 %) was synthesized in two steps starting from dPGOH **1** (M_n = 9.5 kDa, M_w = 11.4 kDa, D = 1.19): first mesylation and then azidation by the procedure reported in the literature ¹. For the functionalization of approximately 15% of the azide groups on dPG(N₃)_{17%} **2** with the controlled amount of propargylated sialic acid derivative, i.e. prop-2-ynyl α -thiosialoside, dPG(N₃)_{17%} **2** (20 mg, 0.040 mmol of azide groups to be functionalized) was dissolved in 5 ml of DMF followed by the addition of prop-2-ynyl α -thiosialoside (21.8 mg, 0.040 mmol). Prop-2-ynyl α -thiosialoside was synthesized using Roy ² and a slightly modified procedure of Ogura ³. The CuSO₄·5H₂O (2.0 mg, 0.008 mmol) was dissolved in 0.2 mL of H₂O and added to the solution of sodium ascorbate (15.9 mg, 0.08 mmol) in 0.5 mL H₂O. The resultant solution of both the salts in water was added drop wise to the solution containing dPG(N₃)_{17%} **2** and prop-2-ynyl α -thiosialoside. The reaction mixture was degassed thoroughly with argon for 5 minutes and then allowed to stir for 12 hours at room temperature under argon atmosphere. Completion of the reaction was monitored by absence of prop-2-ynyl α -thiosialoside on TLC. DMF was evaporated and 2M NaOH (5 ml) was added to the residue and stirred for 2 hours at room temperature. Reaction mixture was neutralized with 1M HCl and dialyzed against water for 3 days using 2 kDa MWCO membrane followed by lyophilization to afford the pure product hPGSAN₃ **3** (32 mg, yield 92%). The pure product was analyzed by GPC, ¹H NMR, and IR.

¹H NMR (500 MHz, D₂O): δ (ppm) = 7.93 (s, 1H, C=CH), 4.55-3.59 [m, SA (H-8, NH, H-7, H-4, H-9, H-5, H-6); SCH₂C=C; and nPG core], 2.77-2.75 (m, SA, H-3e), 1.93 (s, SA, NHAc), 1.75 (SA, H-3a), 1.37 (m, -CH₂- core), 0.85-0.82 (m, -CH₃ core). IR (film): ν = 3303, 2917, 2876, 2102, 1608, 1455, 1435, 1373, 1113, 1077, 953 cm⁻¹. GPC (H₂O): M_n = 19.1 kDa, M_w = 29.6 kDa, D = 1.54.

1.3 LAPEGNH₂ **6**

N₃PEGNH₂ **4** (MW = 5 kDa) (50 mg, 0.01 mmol) was dissolved in THF-H₂O (1:1) (5 mL) followed by addition of *N*-(1,2-Dithiolane-3-pentanoyl)propargylamine⁴ **5** (3.65 mg, 0.015 mmol). The CuSO₄·5H₂O (0.50 mg, 0.002 mmol) was dissolved in 0.2 mL of H₂O and added to the solution of sodium ascorbate (39.6 mg, 0.2 mmol) in 0.5 mL H₂O. The resultant solution of both salts in water was added drop wise to the solution containing N₃PEGNH₂ **4** and *N*-(1,2-Dithiolane-3-pentanoyl) propargylamine **5**. The reaction mixture was degassed thoroughly with argon for 5 minutes and then allowed to stir for 12 hours at room temperature under argon

atmosphere. The progress of the reaction was monitored by IR. THF was evaporated on rotavapor. The aqueous reaction mixture layer was extracted in DCM (50 mL) and washed with H₂O (2 x10 mL). The organic layer was reduced to 2 mL over rotavapor followed by precipitation in diethyl ether to afford the pure product LAPEGNH₂ **6** in quantitative yields. ¹H NMR (500 MHz, D₂O): δ (ppm) = 7.98 (1H, s, -CH=C-), 4.64 (2H, t, *J*=5Hz, triaz-CH₂CH₂O-), 4.49 (2H, s, triaz-CH₂NHCO-), 3.99 (2H, t, *J*=5Hz, triaz-CH₂CH₂O-), 3.88-3.46 (m, -SCH-, PEG backbone), 3.29-3.18 (2H, m, -SCH₂-), 3.02 (2H, brs, -OCH₂CH₂NH₂), 2.52-2.46 (1H, m, -SCH₂CH₂-), 2.32 (2H, t, *J*=5Hz, -NHCOCH₂CH₂-), 2.03-1.96 (1H, m, -SCH₂CH₂-), 1.78-1.58 (4H, m, -NHCOCH₂CH₂CH₂CH₂-), 1.42-1.37 (2H, m, -NHCOCH₂CH₂CH₂CH₂-). IR (CH₃OH): ν (cm⁻¹) = 3312, 2913, 2872, 1955, 1782, 1658, 1439, 1387, 1348, 1088, 947, 840 cm⁻¹. GPC (H₂O): Mn = 5.23 kDa, Mw = 8.87 kDa, D = 1.69.

1.4 dPGSA-PEG-LA **7**

LAPEGNH₂ **6** (10 mg, 0.0018 mmol) was dissolved in dry DMF (1 mL) under argon atmosphere followed by addition of TEA (0.348 μL, 0.0024 mmol) and the solution of bicyclo [6.1.0] non-4-yn-9-ylmethyl (4-nitrophenyl) carbonate (BCN) (0.596 mg, 0.0019 mmol) in dry DMF (0.2 ml). BCN was synthesized as reported before.⁵ The reaction mixture was allowed to stir at room temperature under argon for two hours. The reaction mixture was diluted by adding 10 mL of DMF. Then this reaction mixture was added drop wise to the solution of dPGSAN₃ **3** (3.42 mg, 0.00018 mmol) in DMF (0.5 ml) and H₂O (0.5 ml). The DMF was evaporated and the solution was dialyzed in H₂O using 10-12 kDa MWCO membrane and lyophilized to obtain the product dPGSA-PEG-LA **7** (8 mg, 59% yield). The pure product was analyzed by ¹H NMR, IR, and GPC. ¹H NMR (700 MHz, D₂O): δ (ppm) = 8.04 (brs, C=CH), 4.70-3.09 (m, triaz-CH₂CH₂O-, triaz-CH₂NHCO-, -Oct-CH₂OCONH-, triaz-CH₂CH₂O-, -SCH-, PEG backbone, SA (H-8, NH, H-7, H-4, H-9, H-5, H-6); SCH₂C=C; and hPG core, -SCH₂-), 2.75 (brs, SA, H-3e), 2.37-1.96 (m, Oct, -SCH₂CH₂-, -NHCOCH₂CH₂CH₂CH₂-, SA NHAc, -SCH₂CH₂-, Oct), 1.75 (SA, H-3a), 1.62-0.80 (br, -NHCOCH₂CH₂CH₂CH₂-, -NHCOCH₂CH₂CH₂CH₂-, Oct, -CH₂- core, -CH₃ core). IR (film): ν = 3533, 2876, 2100, 1615, 1455, 1342, 1106, 1060, 982, 842 cm⁻¹. GPC (H₂O): Mn = 25.0 kDa, Mw = 34.9 kDa, D = 1.4.

1.5. Synthesis of multivalent control compound dPGOH-PEG-LA **13**

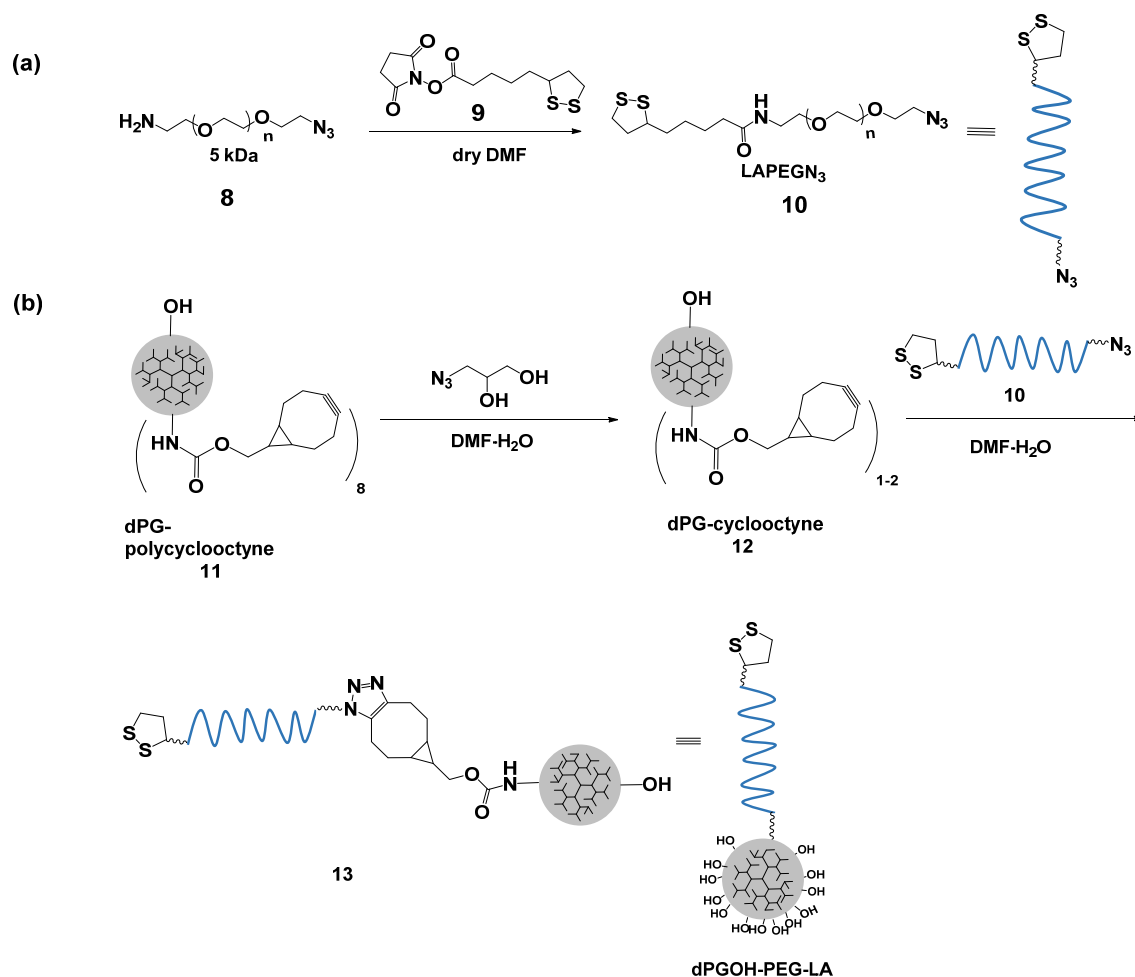


Figure S2. (a) Synthesis of LA-PEG- N_3 multivalent control with the PEG linker dPGOH-PEG-LA 13

1.6. LAPEGN₃ 10

NH₂PEGN₃ **8** (50 mg, 0.01 mmol) was dissolved in dry DMF (3 mL) followed by addition of solution of lipoic acid-NHS ester **9**⁶ (6.06 mg, 0.02 mmol) in dry DMF (1 mL). The reaction mixture was allowed to stir for 12 hours. DMF was evaporated on rota-vapor. The residue was extracted in DCM (50 mL) and washed with H₂O (2x10 mL). The organic layer was reduced to 2 mL over rota-vapor followed by precipitation in diethyl ether to afford the pure product LAPEGN₃ **10** in quantitative yields. ¹H NMR (500 MHz, CDCl₃-CD₂Cl₂): δ(ppm) = 6.35 [s, 1H, -NHCO-], 3.74-3.39 [m, -SCH-, PEG backbone], 3.21-3.10 (m, 2H, -SCH₂-), 2.49-2.44 (1H, m, -SCH₂CH₂-), 2.23 (t, 2H, *J* = 10 Hz, -NHCOCH₂CH₂-), 1.95-1.89 (1H, m, -SCH₂CH₂-), 1.72-1.67 (m 4H, -NHCOCH₂CH₂CH₂CH₂-), 1.50-1.45 (m, 2H, -NHCOCH₂CH₂CH₂CH₂-). IR (DCM): ν = 2878, 2098, 1733, 1651, 1541, 1467, 1341, 1279, 1099 cm⁻¹.

1.7. dPGOH-PEG-LA **13**

hPG-polycyclooctyne (Mw ~ 7216, 10 mg, 0.011 mmol, 8 per hPG) was synthesized starting with dPGOH as reported in literature.⁷ For further use, around 6 cyclooctyne groups were consumed by reaction with azidoglycerol (9.7 mg, 0.0083 mmol) in DMF-H₂O (2 mL, 1:1 ratio) for 2 hours at room temperature. To this reaction mixture in DMF-H₂O added diluted solution of LAPEGN₃ (0.0028 mmol, 0.0152 mg) in DMF (3 mL) drop-wise. The reaction mixture was allowed to stir overnight. DMF was evaporated and the mixture was dialyzed in H₂O using 10-12 kDa MWCO membrane and lyophilized to obtain the product dPGOH-PEG-LA **13** (10 mg, 56 % yield). ¹H NMR (700 MHz, D₂O): δ(ppm) = 4.49-3.18 (m, triaz-CH₂-, -Oct-CH₂OCONH-, -SCH-, PEG backbone, and hPG core, -SCH₂-), 2.55-2.00 (m, Oct, -SCH₂CH₂-, -NHCOCH₂CH₂CH₂CH₂-), 1.81-1.40 (m, -SCH₂CH₂-, -NHCOCH₂CH₂CH₂CH₂-, Oct), 1.30-0.76 (m, Oct, -CH₂- core, -CH₃ core). IR (film): ν = 3369, 2872, 1692, 1658, 1460, 1348, 1105, 945, 849cm⁻¹. GPC (H₂O): Mn = 11.7 kDa, Mw = 18.74 kDa, D = 1.57.

1.8.- ¹H NMR Spectra.

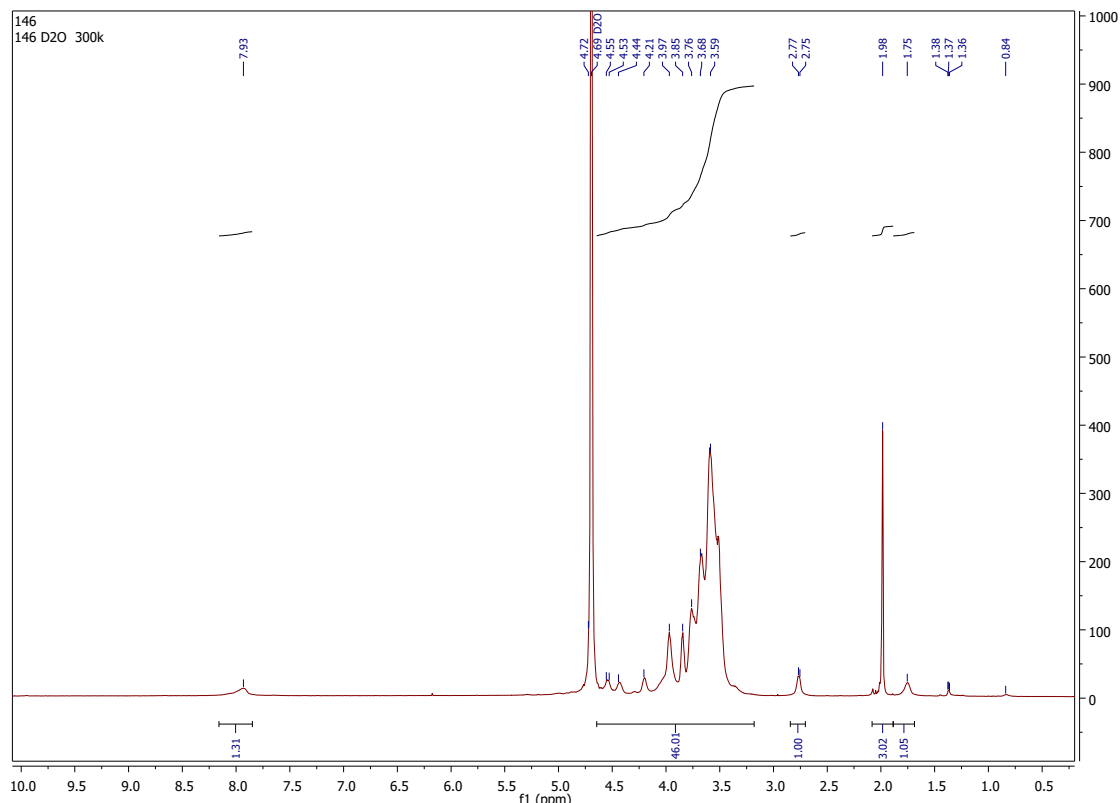


Figure S3a. ¹H NMR (700 MHz, D₂O) of dPGOH-PEG-LA **13**

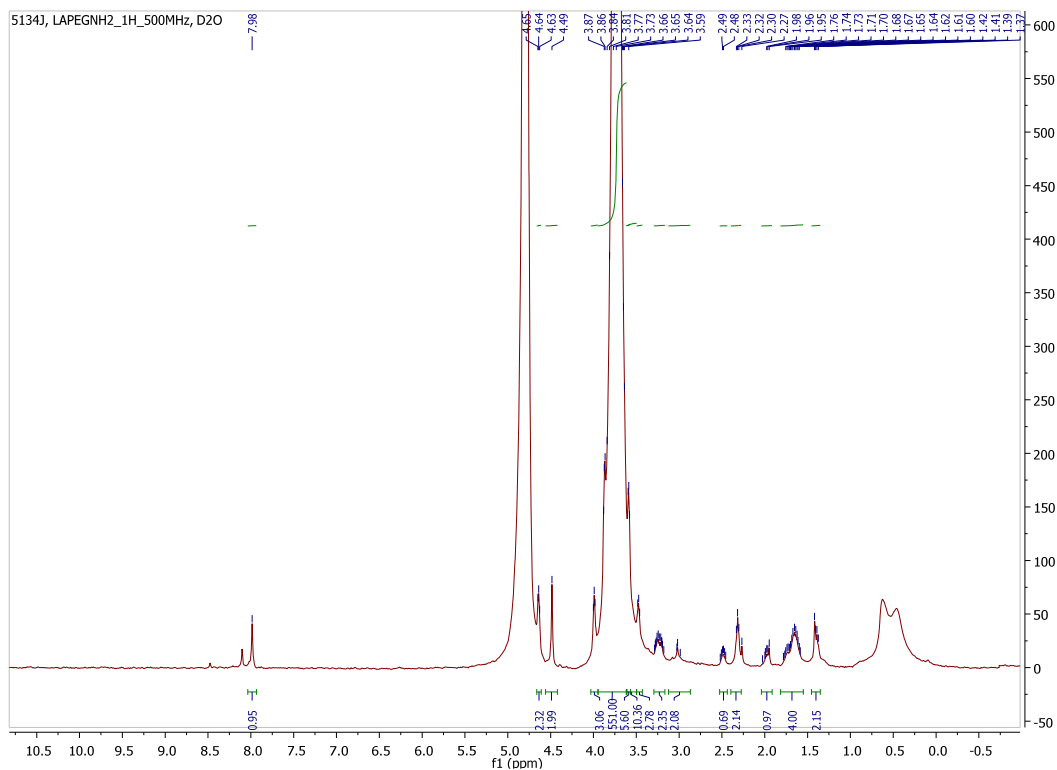


Figure S3b. ^1H NMR (700 MHz, D_2O) of LAPEGNH₂ 6

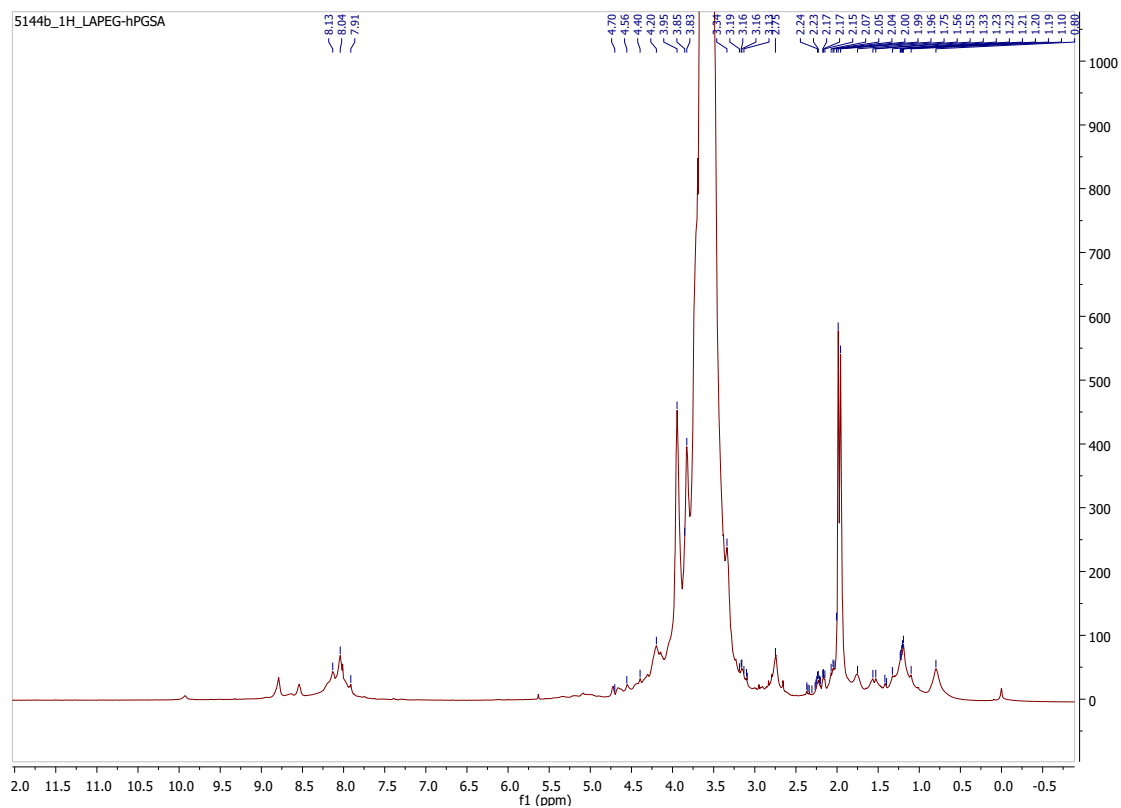


Figure S3c. ^1H NMR (700 MHz, D_2O) of dPGSA-PEG-LA 7

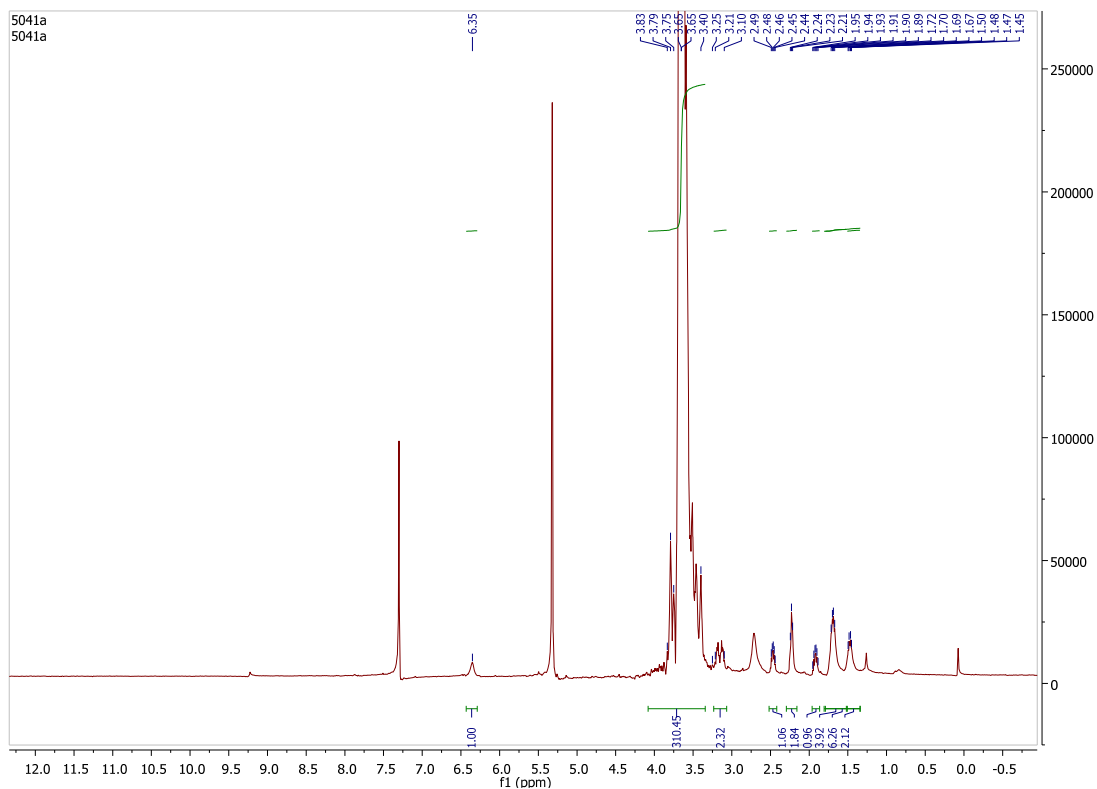


Figure S3d. ^1H NMR (700 MHz, $\text{CDCl}_3\text{-CD}_2\text{Cl}_2$) of LA-PEG- N_3 **10**

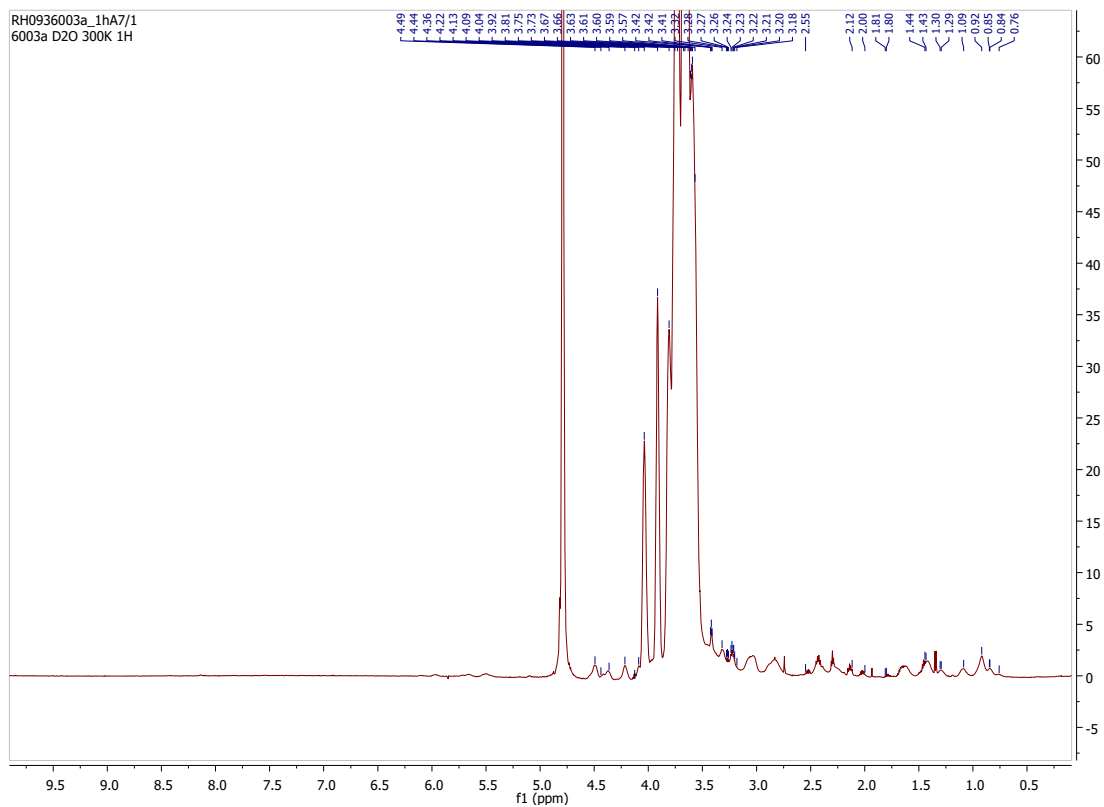


Figure S3e. ^1H NMR (700 MHz, H_2O) of dPGOH-PEG-LA **13**

2. Sample preparation.

2.1 Virus preparation. X31 virus (influenza strain A/Aichi/2/68 H3N2, reassorted with internal segments of A/PuertoRico/8/1934 H1N1), was harvested from allantoic fluid of embryonated chicken eggs. All purification steps were performed on ice or at 4 °C. Virus isolates were clarified upon low speed centrifugation (300 x G, 10 min), followed by an ultracentrifugation step (100,000 x G, 1 h) to obtain virus concentrate. The virus pellet was soaked overnight in TNE buffer (10 mM Tris-HCl, 100 mM NaCl, 1 mM EDTA, pH 7.4), homogenized, loaded on a continuous 20-60 % (w/v) sucrose gradient in TNE buffer and centrifuged for 2 hours at 100,000 x G. Next, the virus band was collected, again pelleted at 100,000 x G and soaked overnight in TNE buffer. On the following day, the virus pellet was dialyzed twice against PBS and the protein concentration was determined via a BCA assay (Thermo Fisher Scientific).

2.2 Immobilization of influenza A virus. Influenza virus was firmly immobilized on self-assembled monolayers (SAM's) of mercaptans on the substrate of gold (1,1,0) plates using a thiol chemistry approach based on a protocol by Friedsam et al.⁸ Gold plates (2x2 cm, from Georg Albert PVD-Beschichtungen, Germany) were first immersed in an aqueous solution of ammonia (30%) and hydrogen peroxide (30%) at 70°C for only 3 minutes, since longer timer could remove the thin Au layer. Then Au plates were rinsed repeatedly with Milli-Q water and immediately immersed in 1 ml of a 99% ethanol solution containing 2.5 mg 16-mercaptohexadecanoic acid and 2 mg 11-mercaptoundecanol and incubated overnight. The mixture of mercapto-terminated alkali thiols creates a self-assembled monolayer (SAM) on the gold surface with slightly unequal surface variations with exposed carboxyl groups. After 24 hours incubation, the surfaces were rinsed repeatedly with 99% ethanol and let it dry. To activate the substrate surface against amino groups, present on the virus surface, the carboxyl-terminated SAM on the gold is reacted in a solution of 1ml MES buffer pH = 6 with a mixture of N-Hydroxysuccinimide (NHS) and 1-Ethyl-3-(3-dimethylaminopropyl) carbodiimide (EDC) in a proportion 1:5 (Sigma-Aldrich). The gold substrates were then incubated with this solution for no longer than 15 minutes and then washed with 1 ml MES buffer and immediately after a 10 µl virus solution (protein conc. > 1.5 mg/ml) was deposited on its center on a previously marked spot. Samples were kept in small circular petri dishes sealed with parafilm to avoid evaporation and incubated for at least an hour before each experiment was perform. After incubation with the virus solution and prior to an experiment the sample was gently rinsed with PBS buffer to remove any unattached material and a 50 µl PBS was deposited again.

Finally, the sample was mounted on the stage of the force robot and a fluid cell was assembled. Therefore, the sample surface was never allowed to dry.

2.3 Immobilization of poly-histidine tagged N2 proteins on NTA surfaces.

Immobilization of poly-histidine tagged proteins on glass substrates coated with a nitrilotriacetic acid layer is a well-known approach to produce highly stable and preferentially oriented protein arrays in biotechnology, and has proven to be a valuable tool in dynamic force spectroscopy studies.⁹⁻¹¹ We used the same approach as reported by Scherer et al.¹². We used commercially available NTA (Nanocs. USA) coated glass substrates. Glass slides were carefully cut into 1.5 x 1.5cm squares with a glass cutter possessing a diamond tip. Immediately after the surfaces were rinsed with milli-Q water to remove any potential dust or glass particles attached to the surface. A 40 μ l solution of NiCl₂ charged with nickel ions was deposited at the center of the NTA glass substrates and incubated for at least 4 hours. After that, the substrate surface was rinsed repeatedly with milli-Q water and a 5 μ l solution of recombinant N2 protein with histag (protein conc. 120 μ g/ml) was placed in the middle and incubated for at least 1 hour. Recombinant Influenza A H3N2 (A/Aichi/2/1968) Neuraminidase with a histag was purchased from Sino Biologicals inc. Protein solutions were prepared in Milli-Q water aliquots immediately after received and stored at -80°C, according to the protocol provided by the company (Sino Biologicals, Inc.). After 1 h incubation with the protein solution, the sample was gently rinsed with PBS and further incubated with a 40 μ l of a 5 mg/ml BSA solution for at least 30 minutes. Incubation with BSA, is applied in order to avoid unspecific binding interactions between our synthetic SA receptors and the NTA coated substrate. Finally, after incubation with the BSA solution, the sample was rinsed again with PBS and mounted on the stage of the Force Robot 300.

2.4 SFM tip functionalization.

A monovalent flexible polyethylene glycol chain (5 kDa PEG) displaying the sialic acid (SA) unit and a dendritic architecture (40 kDa) with 15% SA on its surface were used as receptors to test binding to IAV and N2 proteins. Thiol chemistry was also used for attachment of the sialoside receptors on the SFM tip apex through a lipoic acid (LA) unit at one end. OBL-10 cantilevers from Bruker with gold coated tips were used with spring constants with nominal values of 0.03 and 0.006 N/m. Since receptors were synthesized with a lipoic acid as a terminal group, their attachment to the gold coated tip was direct. 40-50 μ l of a stalk solution (conc: 1 mg/ml) of (SA-PEG-LA) or (hPGSA_{0.15}-PEG-LA) were used to functionalize cantilevers

independently. This small amount was deposited in small wells of a teflon block, where chips were immersed into the solution. Afterwards, the teflon block was placed inside a flask and properly sealed to prevent evaporation. Cantilevers were incubated for at least 8 hours and previous to be mounted to the force robot head, cantilevers were carefully dipped in and out 3 times in Milli-Q water to remove any unattached molecules. Only cantilevers with spring constant 0.03 N/m were used for force measurements. This functionalization method has been widely use in force spectroscopy since allows recording hundreds of cycles without losing of the receptor molecule ⁸.

3. SFM imaging and force spectroscopy.

3.1 Scanning force microscopy. Imaging of the substrate surface was acquired with a Multimode Nanoscope 8 from Bruker in PeakForce mode. To investigate the topography of the substrate coated with IAV virions, SNL-10 cantilevers from Bruker with a nominal radius of 2-12 nm and spring constant of 0.35 N/m were used. Previous cantilever calibration was carried out using the thermal noise method¹³. All measurements were performed in PBS in a fluid cell chamber and sample was prepared as described above. Maximal loading forces during imaging were kept between 200-500 pN to minimize damage on the virus surface and 512 points per line were taken at a 0.7 Hz scan rate. High resolution imaging of protein arrays in NTA glass coated surfaces was performed using ultrasharp SFM tips PeakForce-HIRS B from Bruker with nominal radius 1 nm, maximum 2 nm and spring constant of 0.12 N/m.

3.2 Force Spectroscopy measurements. A Force Robot 300 from JPK (Berlin, Germany) was used during all force spectroscopy measurements. The Force Robot (FR) device, is specially designed for high performance force spectroscopy, which offers a high vertical resolution in acquired measured forces. Force curves were taken using a pre-programmed rectangular grid with an area of 10 x 10 μm^2 and 10 x 10 points. On each point only one force curve was taken, unless specified. Calibration of OBL-10 cantilevers was performed with the thermal tune procedure, using the geometrical dimensions of the cantilever specified by the manufacturer and using the Sader method ¹³. A maximal applied normal force by the tip on the virus surface was set to 100 pN in order to prevent serious mechanical deformation or puncturing the virus envelope. It has already been reported that for sharper tips than the ones used here, forces of up to 500 pN are necessary to perforate the Influenza virus envelope ¹⁴. A constant approach

tip velocity of 0.5 $\mu\text{m/s}$ was used throughout all the measurements, whereas to explore the spectrum of bond rupture, retraction velocities used were 0.1, 0.3, 0.5, 1.0, 2.5, 5 and 10 $\mu\text{m/s}$.

A longer contact time between probe and sample inherently potentiates the formation of more bonds by providing higher time frame to the flexible (SA-PEG-LA) receptors to bind more the H3 or N2 binding pockets on the sample surface. In experiments to test multivalent interactions a dwell time of 700 ms was used. Although measurements were also performed with no dwell time, a minimum contact time is required to allow the tip compress the sample with the given force set point. In the latter case, the tip is immediately retracted, as soon as the tip reaches this set point value, which in our case was always 100 pN. This was used to confirm the reduction in the presence of detected multi-bond rupture, reflected as multiple peaks in histograms of rupture force, and to validate that the first peak in the distribution corresponded to a single bond. For the case of the multivalent receptor, no dwell time was used, since we were interested to increase the probability of detection from binding of single dendritic units and not multiple of these.

For experiments to determine the binding probability BP, the dwell time between tip and sample surface was increased, as follows: 0ms, 20 ms, 50 ms, 100 ms, 300 ms, 700 ms, 1 s, 3 s, 5 s and 10 s. The retraction velocity was 5 $\mu\text{m/s}$. In this study we used the extended version of the freely-jointed chain model (EFJC) provided in the JPKSPM data processing software to describe the extension of a single and multiple PEG chains when stretched in parallel. We used the instantaneous loading rate at rupture force, extracted after a fit to the extensible freely-jointed chain model (EFJC), where we used a Kuhn length of 0.68 nm¹⁵. The use of linear flexible linkers offers several advantages for single bond characterization. It allows for easy identification of individual bond rupture because the extension of the characteristic non-linear pattern observed during retraction before bond breakage, equals the length of the linker used¹⁶. Since PEG linkers can be produced with a low degree of polydispersity (Sigma 0.01 PDI), this can be used as a useful tool for identification of single and multiple bonds. Of central importance in our analysis is the loading rate extracted from the fit to the force-separation curves, because it provides a way to extract the transducer stiffness k_c , which is the combined elastic contribution of cantilever+PEG-Env. Consequently, the transducer stiffness k_c can be obtained for $n = 1, 2, 3$ and 4 bonds as the slope from a linear fit to the obtained data in a plot v vs r , where v is the tip pulling speed and r is the most probable loading rate at rupture.

4. PeakForce imaging results.

4.1 Influenza A virions and protein coated surfaces. As shown in figure S4, both surfaces appear densely coated with a) virions and b) N2 proteins. a) shows a $5 \times 5 \mu\text{m}^2$ scanned region obtained after imaging with conventional SNL tips. Individual influenza A virions can be easily recognized mostly with sphere-like structures including some with filamentous shape, with a height of about 80-110 nm which is consistent with values reported in the literature¹⁷⁻¹⁸. In b) a $500 \times 500 \text{ nm}^2$ scan obtained with ultrasharp PEAKFORCE-HIRS SFM tips shows a surface packed with individual point-like particles with much smaller sizes. Cross section profiles of a virion and a single N2 monomer indicated by arrows in a-b) are given in c-d). Minimal normal forces of 150-200 pN were used to minimize damaging of the protein coat. In figure S5 of SI a direct comparison of the NTA glass topography before and after incubation with N2 monomers clearly confirmed the presence of individual N2 units with a mean height of $8.1 \pm 1.7 \text{ nm}$, measured width of $13.1 \pm 2.1 \text{ nm}$ and inter-protein distance separation of $14.3 \pm 4 \text{ nm}$.

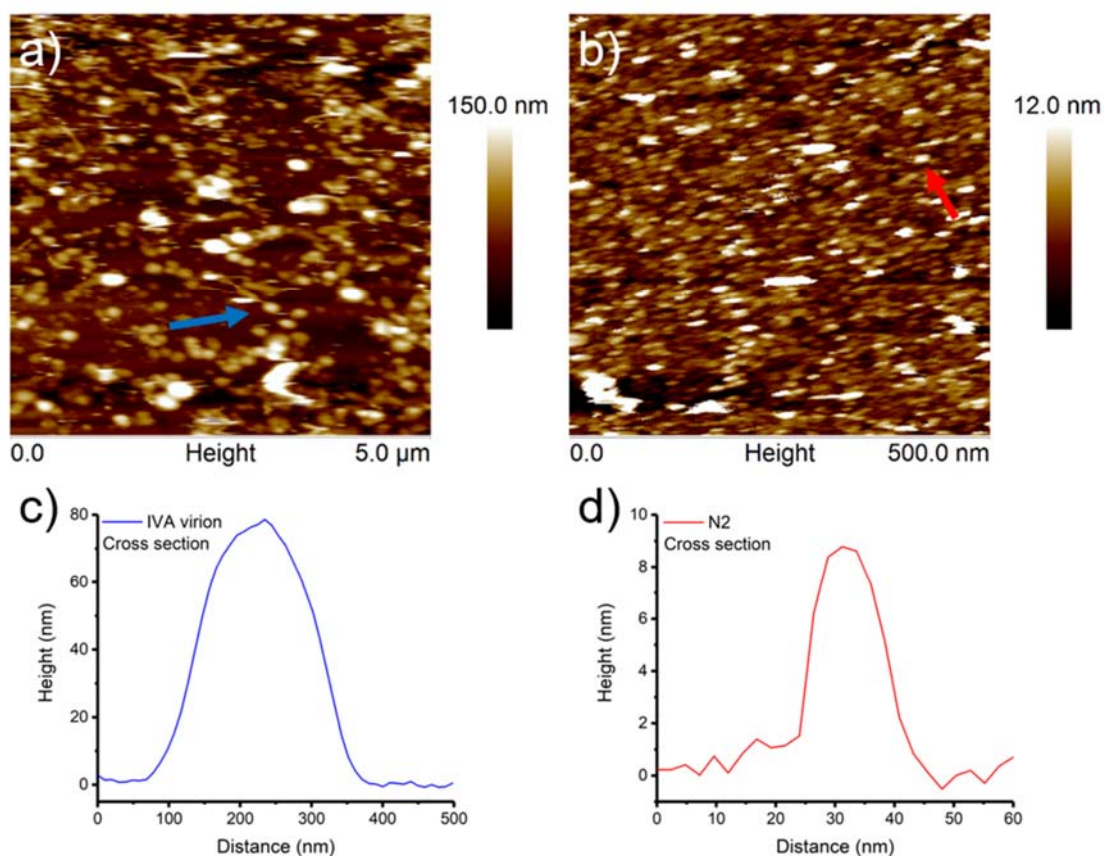


Figure S4. SFM images in PeakForce mode of functionalized substrates with IVA virions and single N2 monomers. In a) IVA virions can be clearly observed as spherical particles covering almost the entire

surface area. b) The surface appears densely packed with very small point-like particles. c) and d) are cross section profiles of a single virus and a single N2 monomer unit indicated by arrows in a) and b).

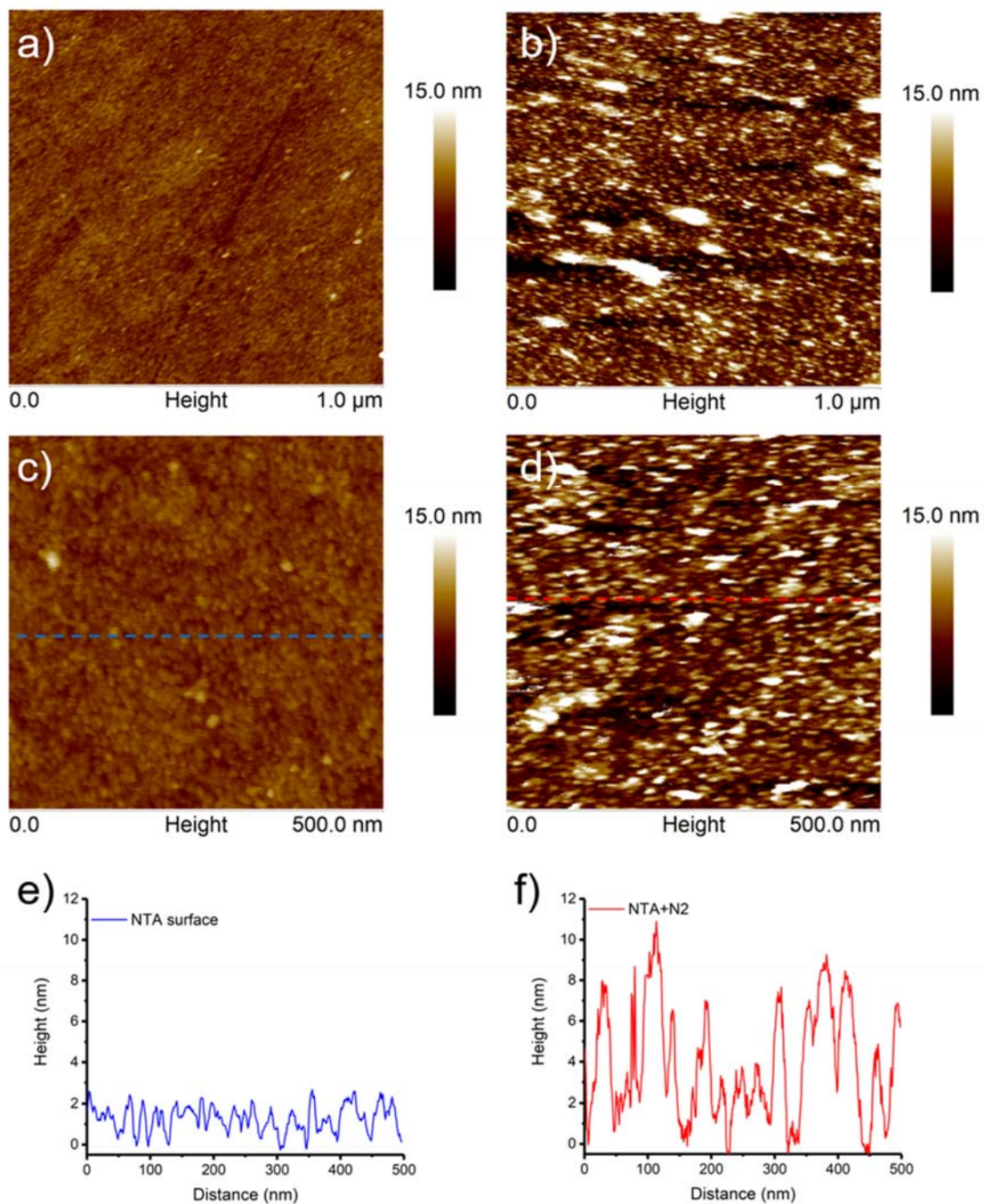


Figure S5. SFM surface topography of protein immobilization on glass-NTA surfaces. In a) glass-NTA after incubation with nickel ions for 2 hours, and b) incubation with N2 for one hour. The drastic change in surface morphology is evident when images are compared with the same z-scale. Individual point-like features can be easily recognized on the surface with dimensions consistent with individual N2

monomers. c) and d) are zoomed images of a) and b) regions for 1 μm and 500 nm scan size. In e) and f) a side view of the surface profile allows to confirm the expected change in surface roughness.

Approximation of monomer “true” width. SFM imaging produces subnanometer accuracy in determination of height differences, but its lateral resolution is limited by the tip size. An estimation of the “true” width for a single N2 protein can be made on geometrical grounds. Considering an average tip opening angle of 20°, a tip radius of 1 nm and the measured values for height and width obtained for N2 proteins, we can use

$$w = w_m - 2 * [(h - r) \tan \alpha + r] \quad (\text{Eq. S1})$$

Where a value of $w \sim 5$ nm is obtained for the width of a single N2 monomer. This dimension is comparable with values obtained when visualizing protein structure of individual protein units as shown below ¹⁹.

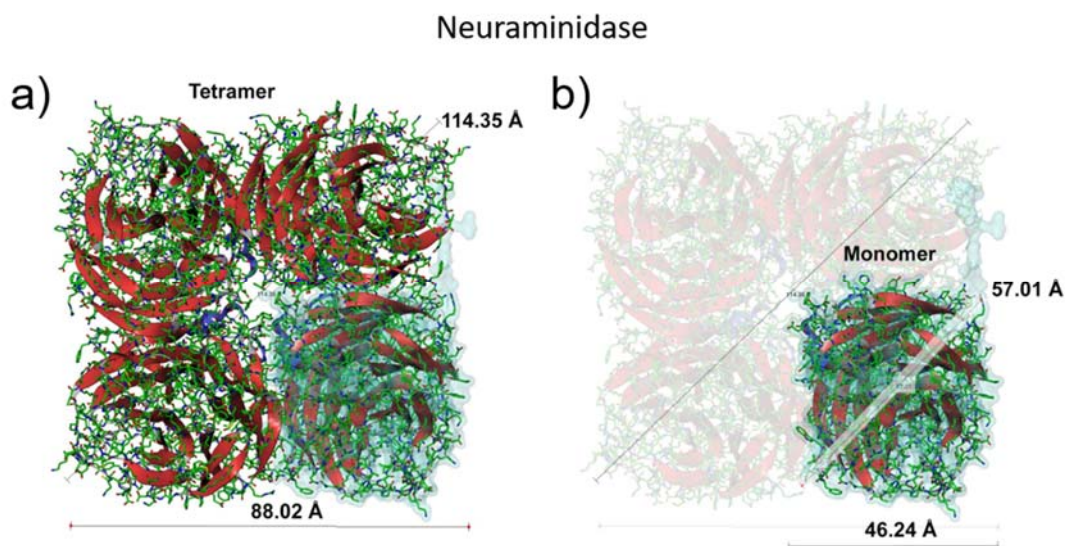


Figure S6. Top view of protein structure of neuraminidase. Full tetrameric a), and single monomeric unit b). As can be seen in b), a lateral distance of a monomeric unit is to be expected between 5 – 6 nm. Figure was prepared using software Amira, version 6.0 (Thermofisher scientific Inc., Waltham (MA), USA).

5. Force spectroscopy.

5.1 Quantification of unbinding forces for single and multiple monovalent-SA receptors with H3 proteins on the influenza A virus and on N2 coated surfaces.

The FDYN model used in this study overcomes the difficulties of the conventional Bell-Evans approach to describe non-linear force spectra, and provides an expression to extract kinetic parameters for single and multi-bonded systems. It also offers an interpretation to inconsistencies previously found in several reported studies related with unrealistic small values obtained for transition state distances ²⁰.

In the FDYN model, the transition state distance χ_β is given in the same way as in the Bell-Evans model, by $\chi_\beta = (k_B T / f_\beta)$, where f_β is the thermal force. However, the relationship between the dissociation rate at equilibrium $k_{off(eq)}$ to that at zero loading applied force k_{off} is given by the following expression

$$k_{off} = \frac{k_{off}(f_{eq})}{e^{\frac{[f_{eq} \cdot \chi_\beta - (1/2) \cdot k_c \cdot \chi_\beta^2]}{k_B T}}} \quad (\text{Eq. S2})$$

where f_{eq} is the equilibrium force and k_c is the stiffness of the force transducer.

Rupture forces

(SA-PEG-LA) - H3

(SA-PEG-LA) - N2

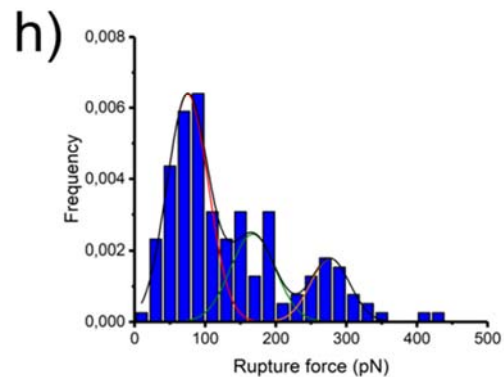
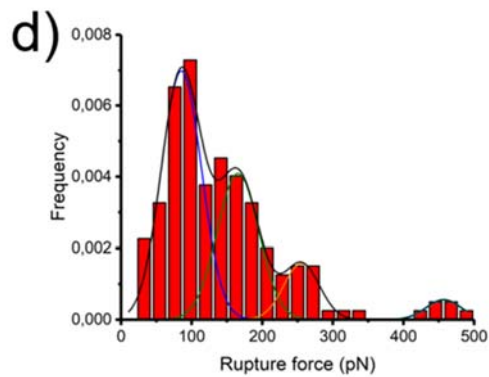
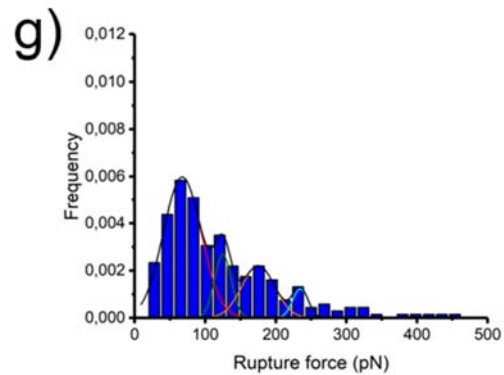
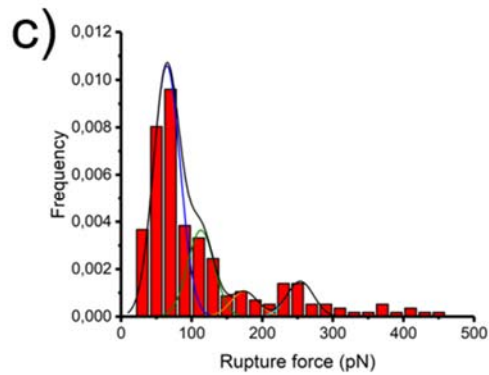
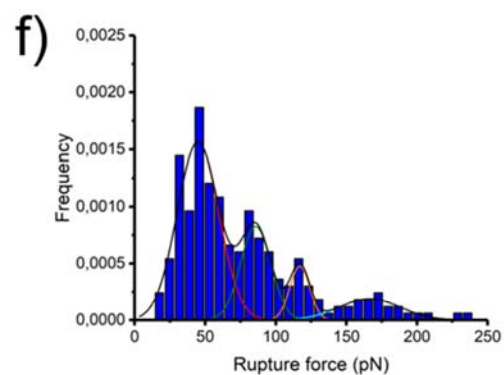
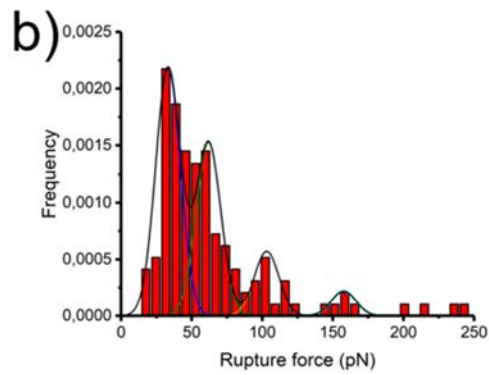
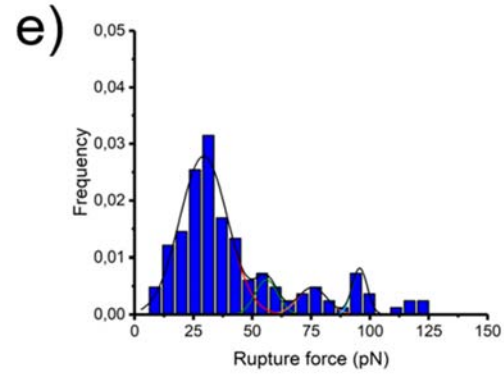
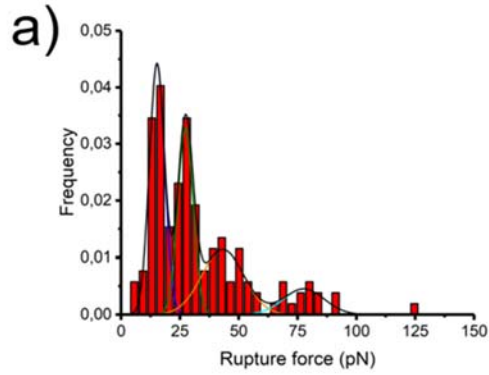


Figure S7. Representative probability density function distributions for rupture forces at increasing loading rates for the unbinding interaction between monovalent SA receptor to a-d) H3 and e-h) N2 proteins. Multiple peaks are fit with multi-Gaussian functions to obtain the most probable rupture force. An expected shift in the most probable rupture forces towards larger loading rates is evident. The difference in rupture forces among sub distributions was evaluated with a non-parametric Kruskal-Wallis test to compare subsequent peak populations. The statistical analysis was performed in OriginPro (2017). In all cases a p value < 0.05 was considered as statistically significant.

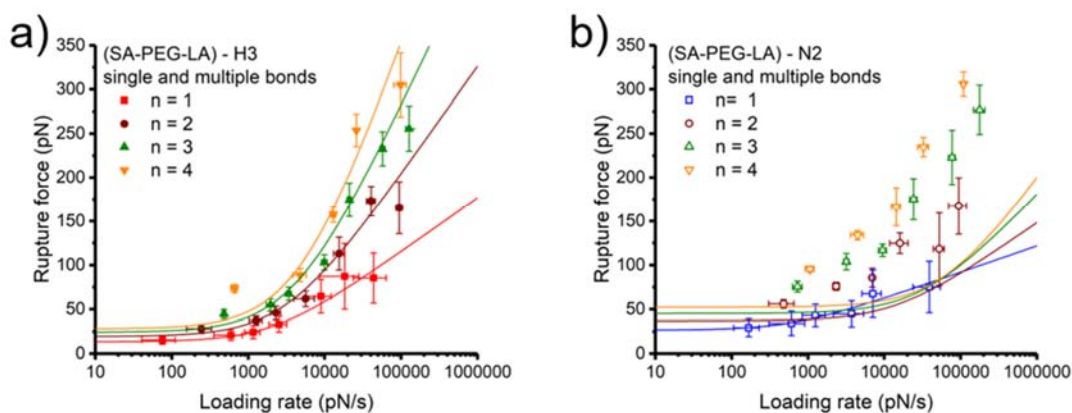


Figure S8. Rupture forces plotted as a function of the loading rate for the unbinding interaction between single and multiple monovalent SA receptors and H3 and N2 proteins. The FDYN model is used to fit the force spectra with equation (1) from the main text. Only data for the single bond (left: solid red squares, and right: open blue squares) is fitted with f_{eq} , f_{β} and $k_{off(eq)}$ as free parameters. Other data is fitted for $n = 2, 3$ and 4 bonds using the parameters for f_{β} and $k_{off(eq)}$ obtained for the single bond (see table 1a-b from main text) and f_{eq} is approximated from $f_{eq}(n) = n^{1/2} f_{eq}(n = 1)$. As can be observed, the force spectra are also well described for SA-H3, but deviations at in the low regime of loading rates are evident as n increases. An obvious discrepancy is obtained for values beyond the single bond for the case of SA-N2. Bars represent standard deviations from distributions of most probable rupture force and loading rates.

5.2 Single apparent bond (SAB).

In this section we provide obtained parameters with the FDYN model when the multivalent connection is described as a single apparent stiff bond. In SMFS experiments, is common practice that the experimenter test bond breakage blindly, having force-separation curves as the only outcome from the unbinding interaction. Unless specific additional information about the investigated system is given, like certain criteria to account for measurement of single and multiple bonds, there is a significant risk for misinterpretation of the obtained data. These

situations, have lead in the past to report unrealistic bond kinetic parameters, particularly extremely small transition state distances.

If we consider that the force spectra obtained for $n = 2$, $n = 3$ and $n = 4$ can be approximated as the result of the measurement of independent individual stronger bonds, then we can apply equation (1) from main text with $n = 1$, and fit f_{eq} , f_{β} and $k_{off(eq)}$ as independent free parameters for each set of force spectra. Results from fits to experimental data are provided in figure S9.

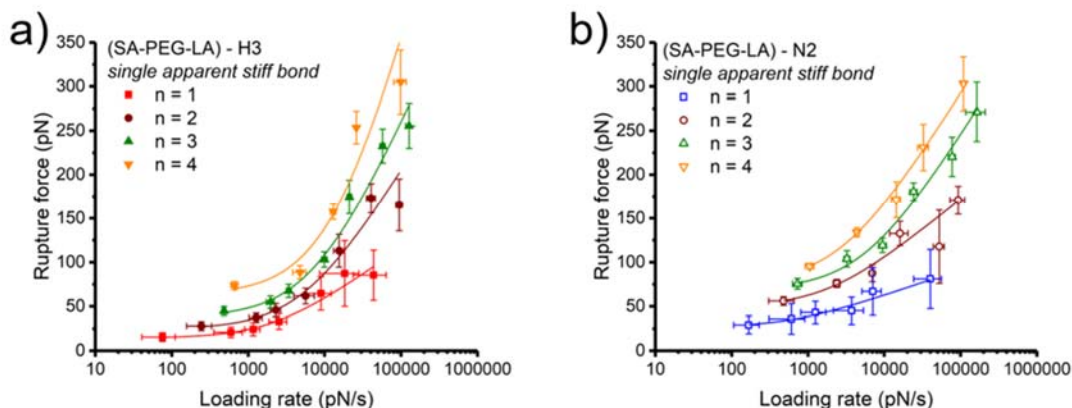


Figure S9. Force spectroscopy data fitted with the FDYN model under the assumption that each set represents the spectrum of rupture forces for independent single bonds. Bars represent standard deviations from distributions of most probable rupture force and loading rates.

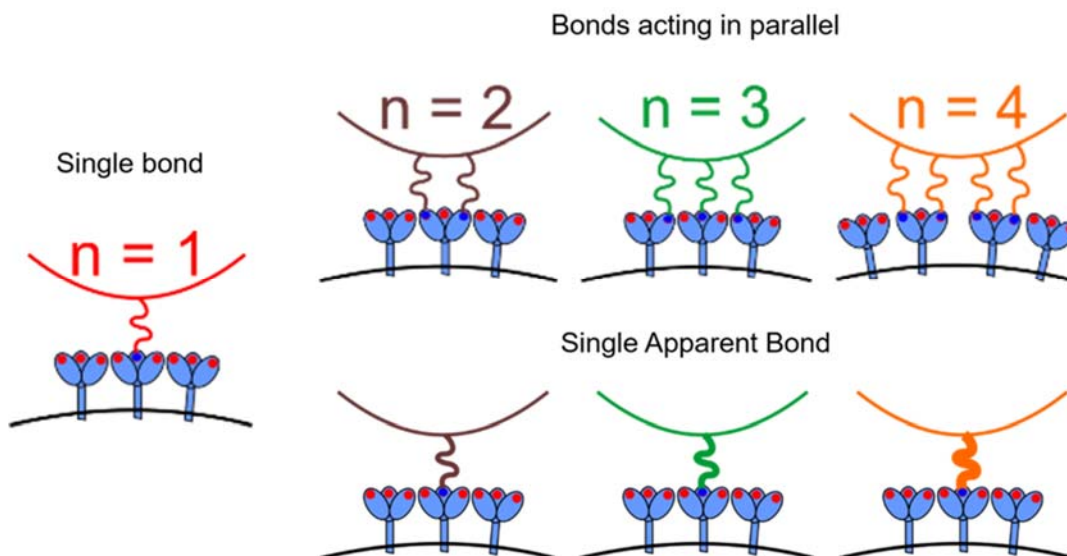


Figure S10. Schematic representation of the single apparent bond (SAB). As shown in the drawing, except from $n = 1$, the subsequent multivalent attachments (comparison top-bottom) can be regarded

as the rupture force of single but stronger bonds. As shown in figure 4a-b, rupture of multiple bonds not only resulted in an increase of the magnitude of the measured force, but also in the stiffness of the transducer or connection, reflected as a steeper slope before rupture.

In this approximation, an accurate determination of the dissociation rates requires individual consideration of the connection stiffness k_c (Eq. S2 from SI) for each consecutive bond. As shown in Figure S11 a-b, k_c is calculated from the slope of a linear fit to v vs r plot, where v is the pulling speed and r is the most probable loading rate at rupture. As pointed out by Friddel and coworkers, stretching of multiple bonds connected in parallel produces stiffer connections generated by the number of molecular tethers mediating the force between the force probe (Cantilever+nPEG+Env) and the bond, as shown in figure S10. They showed that direct analysis of a multi-bond system with the equation for the single bond results in n-times reduced transition states distances χ_β . Our results for the case of SA-H3 and SA-N2 show indeed this outcome for the obtained transition state distances, as shown below in Table S1.

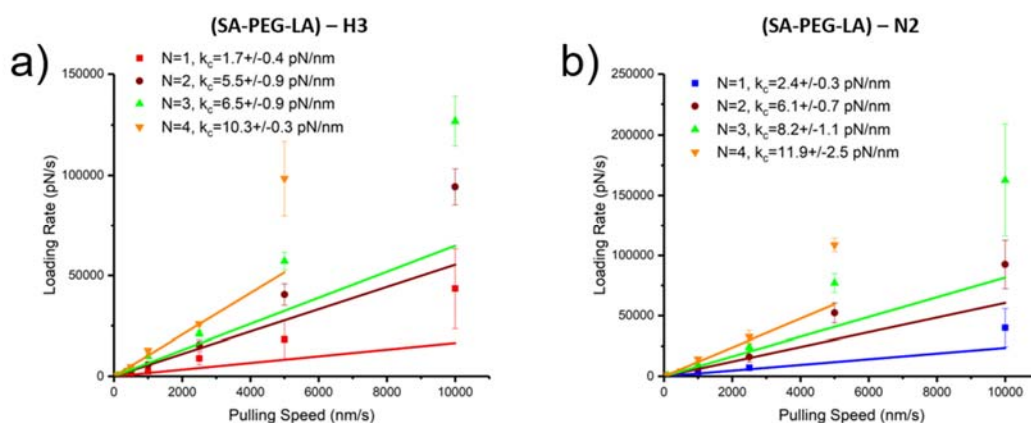


Figure S11. Plots of pulling speed vs loading rate for a) SA-H3 and b) SA-N2, to obtain the transducer stiffness k_c in each configuration. Vertical bars represent standard deviations from distributions of most probable loading rates.

Table S1. Kinetic parameters obtained with FDYN model for single and multiple bonds between monovalent-SA receptor and both spike proteins H3 and N2 of the IAV, when each set of force spectra is fitted individually with equation (1) from text, with $n = 1$ under the assumption of a single apparent bond. Propagation of the error us used to determine the uncertainties in the calculated values.

SA – H3						
# of bonds	f_{eq} (pN)	F_{β} (pN)	$k_{off}(f_{eq})$ (s ⁻¹)	k_{off} (s ⁻¹)	X_{β} (nm)	ΔG (k _B T)
n = 1	14.6±1.7	26.8±5.9	47.8±13.4	27.9±7.9	0.15±0.03	15.2±5.2
n = 2	24.8±4.6	61.6±16.4	51.4±18.7	34.5±8.6	0.06±0.01	13.6 ± 7.8
n = 3	37.9±5.3	83.8±16.5	50.5±13.9	32.2±8.9	0.049±0.01	26.8 ± 7.5
n = 4	63.5±13.4	139.4±104.7	55.9±30.9	35.5±19.8	0.029±0.02	47.6±20.1
SA – N2						
# of bonds	f_{eq} (pN)	F_{β} (pN)	$k_{off}(f_{eq})$ (s ⁻¹)	k_{off} (s ⁻¹)	X_{β} (nm)	ΔG (k _B T)
n = 1	26.9±1.9	13±5	28.7±27.1	3.7± 3.5	0.3 ± 0.1	36.7±14.4
n = 2	49.4±7.5	30.7±7.5	34.1±20.7	6.9±4.2	0.13±0.03	48.7±15.8
n = 3	69.0±8.4	60.3±16.4	52.1±23.0	16.7±7.4	0.07±0.02	70.6±19.3
n = 4	76.5±4.3	60.1±7.4	26.2±5.8	7.4±1.6	0.07±0.01	59.8±14.3

It can be seen that values obtained for the transition state distances χ_{β} reduces significantly as n increases (in bold). However, they noticed that rupture force spectra that results from a multi-bond system can be described with the same mathematical function as the single bond case, if the following apparent force scale is taken into account.

$$f_{\beta}^{app} = n \cdot f_{\beta} = \left(\frac{k_B T}{\chi_{\beta} / n} \right) \quad (\text{Eq. S3})$$

where for the multi-bond case we see that n factors inversely with the transition state distance for the single bond. Taking this into consideration, a correction to the transition state distances can be made as shown in table S2.

Table S2. Apparent transition state distances for the unbinding interaction between monovalent-SA receptor and H3 and N2 proteins. It can be observed that obtained values for χ_β are in close agreement with that of the single bond. Propagation of the error us used to determine the uncertainties in the calculated values.

Number of bonds	SA-H3	SA-N2	SA-H3	SA-N2	SA-H3	SA-N2
	χ_β (nm)	χ_β (nm)	k_{off} (s ⁻¹)	k_{off} (s ⁻¹)	Δt (s)	Δt (s)
n = 1	0.15±0.03	0.3 ± 0.1	27.9±7.9	3.7± 3.5	0.036	0.27
n = 2	0.13±0.02	0.27±0.03	23.3±8.5	1.4±0.9	0.042	0.71
n = 3	0.15±0.01	0.2±0.02	13.2±3.7	1.8±0.8	0.075	0.55
n = 4	0.12±0.02	0.27±0.01	9.2±5.1	0.18±0.04	0.11	5.55

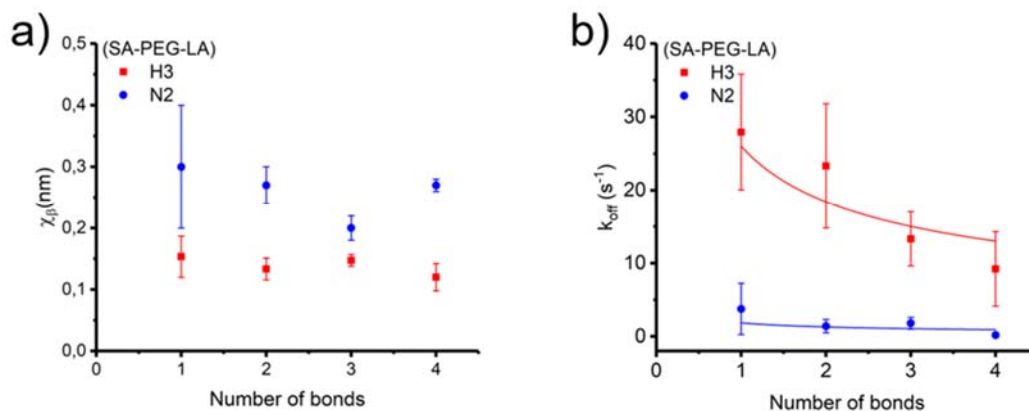


Figure S12. Kinetic bond parameters plotted as the function of the valency when the FDYN model is applied under the assumption of a single apparent bond. Correction to an apparent force scale have been made. In a) it can be observed that values obtained for χ_β for the multi-bond system remain almost constant and close to the value for the single bond case ($n = 1$), which validates our assumption of a set of n identical bonds in parallel. Comparison of obtained dissociation rate constants k_{off} as a function of n in b), show that the single apparent bond approximation produces consistent results with the predictions by the theoretical expression provided by equation (2) for the model of n bonds connected in parallel. The data is fitted with the same function $k_{\text{off}}(n) = k_{\text{off}}(n=1) n^{-1/2}$ as that provided in Figure 5c, and shows that this approximation provides a consistent description for the dissociation rate. A trend towards larger values of bond life-time Δt for the multivalent complex can be observed in table S1ab particularly for $n= 4$. Propagation of the error us used to determine the uncertainties in the calculated values.

5.3 Quantification of unbinding forces for multivalent-SA receptors with influenza A virus and N2 proteins.

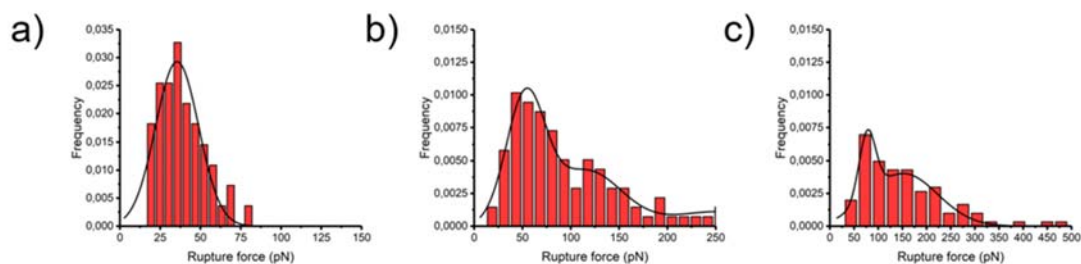


Figure S13. Representative distributions with single and multi-Gaussian fits obtained for the interaction between multivalent-SA receptor and H3 proteins of IAV for increasing retraction speeds. a) 0.1 $\mu\text{m/s}$, b) 2.5 $\mu\text{m/s}$ and c) 10 $\mu\text{m/s}$.

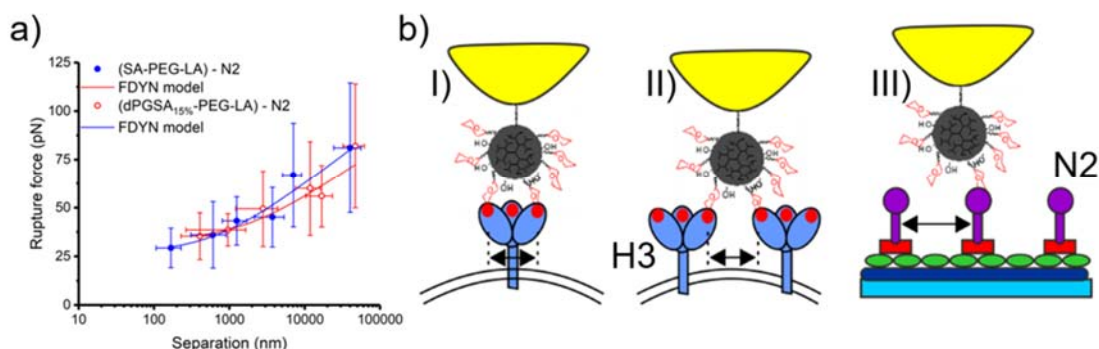


Figure S14. Binding of multivalent SA receptor to N2 proteins. In a), comparison of force spectroscopy data for the binding interaction between monovalent and multivalent SA receptor with a surface coated with N2 monomers. Data is fitted with the FDYN model and we obtained reduced chi-squared values of $\chi^2 = 0.1$ for monovalent-N2 and $\chi^2 = 0.08$ for multivalent-N2. Obtained t -test values where $p < 0.05$ was considered significant showed that only 40% of the compared rupture forces were significant, meanwhile all tested loading rates showed a significant difference. obtained in the kinetic parameters suggests that the multivalent SA receptor binds with a single SA unit to the N2 binding pocket. A higher protein surface density on the IAV allows bridging among binding sites on H3 proteins. Inter and intra-protein binding might occur as shown in Figure b, I and II. On the NTA surface, a larger inter-protein distances among N2 monomers prevent multivalent binding to occur, as depicted in III. Bars represent standard deviations from distributions of most probable rupture force and loading rates.

References:

1. Bhatia, S.; Lauster, D.; Bardua, M.; Ludwig, K.; Angioletti-Uberti, S.; Popp, N.; Hoffmann, U.; Paulus, F.; Budt, M.; Stadtmüller, M.; Wolff, T.; Hamann, A.; Böttcher, C.; Herrmann, A.; Haag, R. Linear polysialoside outperforms dendritic analogs for inhibition of influenza virus infection in vitro and in vivo. *Biomaterials* **2017**, *138*, 22-34.
2. Gan, Z.; Roy, R. Sialoside clusters as potential ligands for siglecs (sialoadhesins). *Can. J. Chem.* **2002**, *80* (8), 908-916.
3. Ogura, H.; Furuhashi, K.; Itoh, M.; Shitori, Y. Syntheses of 2-O-glycosyl derivatives of N-acetyl-d-neuraminic acid. *Carbohydr. Res.* **1986**, *158*, 37-51.
4. Garin, D.; Oukhatar, F.; Mahon, A. B.; Try, A. C.; Dubois-Dauphin, M.; Laferla, F. M.; Demeunynck, M.; Sallanon, M. M.; Chierici, S. Proflavine derivatives as fluorescent imaging agents of amyloid deposits. *Bioorg. Med. Chem. Lett.* **2011**, *21* (8), 2203-2206.
5. Dommerholt, J.; Schmidt, S.; Temming, R.; Hendriks, L. J. A.; Rutjes, F. P. J. T.; van Hest, J. C. M.; Lefeber, D. J.; Friedl, P.; van Delft, F. L. Readily accessible bicyclononynes for bioorthogonal labeling and three-dimensional imaging of living cells. *Angew. Chem. Int. Ed.* **2010**, *49* (49), 9422-9425.
6. Liu, W.; Howarth, M.; Greytak, A. B.; Zheng, Y.; Nocera, D. G.; Ting, A. Y.; Bawendi, M. G. Compact biocompatible quantum dots functionalized for cellular imaging. *J. Am. Chem. Soc.* **2008**, *130* (4), 1274-1284.
7. Dey, P.; Bergmann, T.; Cuellar-Camacho, J. L.; Ehrmann, S.; Chowdhury, M. S.; Zhang, M.; Dahmani, I.; Haag, R.; Azab, W. Multivalent Flexible Nanogels Exhibit Broad-Spectrum Antiviral Activity by Blocking Virus Entry. *ACS Nano* **2018**, *12* (7), 6429-6442.
8. Friedsam, C.; Bécares, A. D. C.; Jonas, U.; Gaub, H. E.; Seitz, M. Polymer Functionalized AFM tips for Long-Term Measurements in Single-Molecule Force Spectroscopy. *Chemphyschem* **2004**, *5* (3), 388-393.
9. Kienberger, F.; Kada, G.; Gruber, H. J.; Pastushenko, V. P.; Riener, C.; Trieb, M.; Knaus, H.-G.; Schindler, H.; Hinterdorfer, P. Recognition Force Spectroscopy Studies of the NTA-His6 Bond. *Single Mol.* **2000**, *1* (1), 59-65.
10. Lata, S.; Reichel, A.; Brock, R.; Tampé, R.; Piehler, J. High-Affinity Adaptors for Switchable Recognition of Histidine-Tagged Proteins. *J. Am. Chem. Soc.* **2005**, *127* (29), 10205-10215.
11. Wu, C.-C.; Reinhoudt, D. N.; Otto, C.; Velders, A. H.; Subramaniam, V. Protein Immobilization on Ni(II) Ion Patterns Prepared by Microcontact Printing and Dip-Pen Nanolithography. *ACS Nano* **2010**, *4* (2), 1083-1091.
12. Reiter-Scherer, V.; Cuellar-Camacho, J. L.; Bhatia, S.; Haag, R.; Herrmann, A.; Lauster, D.; Rabe, J. P. Force Spectroscopy Shows Dynamic Binding of Influenza Hemagglutinin and Neuraminidase to Sialic Acid. *Biophys. J.* **2019**, *116* (6), 1037-1048.
13. Sader, J. E.; Chon, J. W. M.; Mulvaney, P. Calibration of rectangular atomic force microscope cantilevers. *Rev. Sci. Instrum.* **1999**, *70* (10), 3967-3969.
14. Li, S.; Eghiaian, F.; Sieben, C.; Herrmann, A.; Schaap, I. A. T. Bending and puncturing the influenza lipid envelope. *Biophys. J.* **2011**, *100* (3), 637-645.
15. Liese, S.; Gensler, M.; Krysiak, S.; Schwarzl, R.; Achazi, A.; Paulus, B.; Hugel, T.; Rabe, J. P.; Netz, R. R. Hydration Effects Turn a Highly Stretched Polymer from an Entropic into an Energetic Spring. *ACS Nano* **2017**, *11* (1), 702-712.
16. Hinterdorfer, P.; Dufrêne, Y. F. Detection and localization of single molecular recognition events using atomic force microscopy. *Nat. Methods* **2006**, *3* (5), 347-355.
17. Li, S.; Sieben, C.; Ludwig, K.; Höfer, C. T.; Chiantia, S.; Herrmann, A.; Eghiaian, F.; Schaap, I. A. T. pH-Controlled two-step uncoating of influenza virus. *Biophys. J.* **2014**, *106* (7), 1447-1456.
18. Schaap, I. A. T.; Eghiaian, F.; des Georges, A.; Veigel, C. Effect of Envelope Proteins on the Mechanical Properties of Influenza Virus. *J. Biol. Chem.* **2012**, *287* (49), 41078-41088.

19. Smith, B. J.; Colman, P. M.; Von Itzstein, M.; Danylec, B.; Varghese, J. N. Analysis of inhibitor binding in influenza virus neuraminidase. *Protein Sci.* **2001**, *10* (4), 689-696.
20. Friddle, R. W.; Noy, A.; De Yoreo, J. J. Interpreting the widespread nonlinear force spectra of intermolecular bonds. *Proc. Nat. Acad. Sci. U.S.A.* **2012**, *109* (34), 13573-13578.